Earth and Planetary Science Letters 430 (2015) 209–223

Contents lists available at ScienceDirect

Earth and Planetary Science Letters

www.elsevier.com/locate/epsl

Asteroid impact vs. Deccan eruptions: The origin of low magnetic susceptibility beds below the Cretaceous–Paleogene boundary revisited

Alexandra Abrajevitch [a,*], Eric Font [b], Fabio Florindo [c], Andrew P. Roberts [d]

[a] Institute of Tectonics and Geophysics, Kim-Yu-Chen 65, Khabarovsk 680000, Russia
[b] IDL-FCUL, Instituto Dom Luís, Faculdade de Ciências, Universidade de Lisboa, Campo Grande, 1749-016, Portugal
[c] Istituto Nazionale di Geofisica e Vulcanologia, Via di Vigna Murata 605, 00143-Rome, Italy
[d] Research School of Earth Sciences, Australian National University, Canberra, Acton 0200, Australia

ARTICLE INFO

Article history:
Received 21 May 2015
Received in revised form 16 August 2015
Accepted 19 August 2015
Available online xxxx
Editor: M. Frank

Keywords:
rock magnetism
Cretaceous–Paleogene boundary
extinction
magnetotactic bacteria

ABSTRACT

The respective roles of an asteroid impact and Deccan Traps eruptions in biotic changes at the Cretaceous–Paleogene (K–Pg) boundary are still debated. In many shallow marine sediments from around the world, the K–Pg boundary is marked by a distinct clay layer that is often underlain by a several decimeter-thick low susceptibility zone. A previous study of the Gubbio section, Italy (Lowrie et al., 1990), attributed low magnetization intensity in this interval to post-depositional dissolution of ferrimagnetic minerals. Dissolution was thought to be a consequence of downward infiltration of reducing waters that resulted from rapid accumulation of organic matter produced by mass extinctions after the K–Pg event. We compare the magnetic properties of sediments from the Gubbio section with those of the Bidart section in southern France. The two sections are similar in their carbonate lithology and the presence of a boundary clay and low susceptibility zone. When compared to background Cretaceous sediments, the low susceptibility zone in both sections is marked by an absence of biogenic magnetite, a decrease in total ferrimagnetic mineral content, and a preferential loss of magnetite with respect to hematite – features that are consistent with reductive dissolution. However, unlike the Gubbio section, where the low susceptibility zone starts immediately below the boundary clay, the low susceptibility zone and the clay layer at Bidart are separated by a ~4-cm carbonate interval that contains abundant biogenic magnetite. Such separation casts doubt on a causal link between the impact and sediment bleaching. More likely, the low susceptibility layer marks a different environmental event that preceded the impact. An episode of increased atmospheric and oceanic acidity associated with Deccan Traps volcanism that occurred well before the K–Pg impact is argued here to account for the distinct magnetic properties of the low susceptibility intervals.

1. Introduction

The Cretaceous–Paleogene boundary (K–Pg) marks the end of the Mesozoic Era and the beginning of the Cenozoic Era, is characterized globally by a major mass extinction event (e.g., Raup and Sepkoski, 1986; MacLeod et al., 1997), and is one of the best-studied time intervals in Earth history. Two major catastrophic events, the Chicxulub asteroid impact and the Deccan Traps eruptions, have been implicated in complex climatic changes that culminated in the mass extinction, but their respective roles are still much debated (e.g., Schulte et al., 2010; Courtillot and Fluteau, 2010; Renne et al., 2013; Keller, 2014).

Since discovery of an iridium (Ir) and other platinum-group elements anomaly at the K–Pg boundary clay at Gubbio, Italy, the impact hypothesis formulated by Alvarez et al. (1980) has become firmly entrenched in the popular and scientific literatures. In addition to its great imaginative appeal, with dinosaurs wiped out in a single day in a ball of fire caused by a meteorite impact, the impact hypothesis is supported by the presence of impact-derived microtektites, shocked quartz grains and Ni-rich spinels in K–Pg boundary deposits (e.g., Sharpton et al., 1993; Robin et al., 1993; Smit, 1999; Arenillas et al., 2006), as well as by discovery of a giant impact crater on the Yucatán Peninsula, Mexico (Hildebrand et al., 1991; Gulick et al., 2013). As recently as 2010, an international panel of scientists singled out the Chicxulub impact as the ultimate cause of the end-Cretaceous extinction (Schulte et al., 2010).

Despite evidence for an end-Cretaceous bolide impact, this hypothesis fails to explain the selective nature of the K–Pg mass

* Corresponding author.
E-mail address: alexandra.abrajevitch@gmail.com (A. Abrajevitch).

http://dx.doi.org/10.1016/j.epsl.2015.08.022
0012-821X/

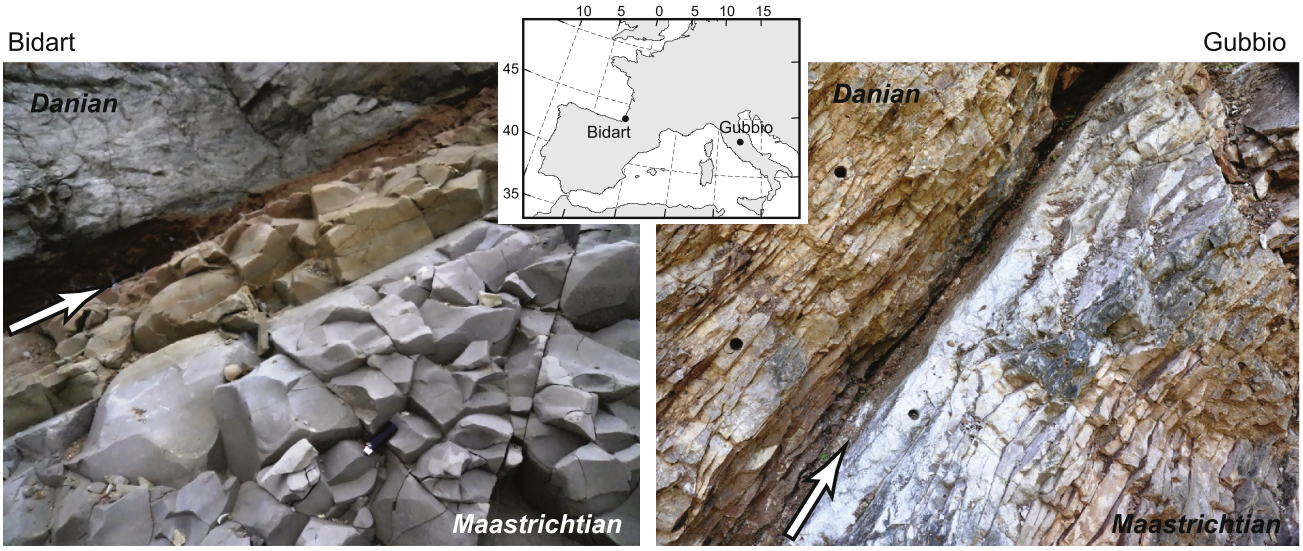

Fig. 1. Location and field photographs of the Gubbio and Bidart sections. Arrows indicate the base of the boundary clay layer (formal K–Pg boundary). Scales: disposable ~8-cm cigarette lighter (Bidart) and standard ~2.5-cm diameter paleomagnetic drill-cores (Gubbio).

extinction (Archibald and Bryant, 1990; Keller et al., 1996), its geographically variable patterns (e.g., Keller et al., 1993), and a long-term decline in species diversity prior to the K–Pg boundary (e.g., Marshall and Ward, 1996; MacLeod et al., 1997). Mounting evidence that the end-Cretaceous mass extinction was the result of a complex multi-event catastrophe brought about by the coincidence of major climate fluctuations, volcanism and impacts (Keller, 2014) warrants re-evaluation of the impact hypothesis to explain geological observations around the K–Pg transition interval.

The Global Stratotype Section and Point for the K–Pg boundary was selected by the International Commission on Stratigraphy (ICS) at a section near El Kef, Tunisia. The boundary is primarily defined by a lithologic marker – the boundary clay layer with the 2–3 mm oxidized layer at the base that contains a peak of Ni-rich spinel and an Ir anomaly (Molina et al., 2006). Formally, the K–Pg boundary is placed at the base of the boundary clay layer. According to the ICS definition, Ni-rich spinels and an Ir anomaly in the boundary clay are interpreted as impact ejecta features, so formation of the boundary clay is regarded as a consequence of an asteroid impact (Molina et al., 2006).

In many marine sedimentary sequences, the distinctive boundary clay layer is often underlain by a several decimeter-thick zone with low magnetic susceptibility (e.g., Lowrie et al., 1990; Ellwood et al., 2003). This low susceptibility interval roughly corresponds to the CF1 and CF2 biozones that contain dramatic changes in planktic foraminifera, nanno- and macro-fossils that led to the K–Pg boundary extinction and is roughly coincident with the timing of the Deccan Phase-2 eruptions (Thibault and Gardin, 2010; Keller et al., 2010; Keller, 2014; Gertsch et al., 2011; Font et al., 2014; Schoene et al., 2015). A widely-accepted interpretation for the origin of the low susceptibility zone (LSZ) was proposed by Lowrie et al. (1990) for the Gubbio section in Italy. These authors attributed the low magnetization intensity in the white beds to post-depositional dissolution of ferrimagnetic minerals. Dissolution is thought to be a consequence of downward infiltration of reducing waters that resulted from rapid organic matter accumulation produced by mass extinctions after the hypothesized impact. In this study, we test this interpretation by comparing the magnetic properties of sediments from the Gubbio section, central Italy, to those from another well-studied carbonate section that contains the complete K–Pg transition interval, the Bidart section in France.

2. Sampling

2.1. Gubbio section

The classic K–Pg transition interval occurs within a well-exposed section of the Scaglia Rossa Formation in Bottaccione gorge near the town of Gubbio in the Umbrian Apennines, Italy (Fig. 1). The Scaglia Rossa Formation mostly consists of bedded red and pink limestones, with Maastrichtian sediments having lighter shades of red compared to Danian sediments. An approximately 0.50-m-thick interval composed of white limestone occurs just below the K–Pg boundary (Fig. 1). The boundary is marked by a 1–2-cm-thick boundary clay layer with anomalously high Ir concentration (Alvarez et al., 1980) and shock-metamorphosed minerals (Montanari et al., 1983; Crocket et al., 1988) that have been interpreted as providing evidence for collision with a large Earth-crossing asteroid (Alvarez et al., 1980).

The distinct bedded appearance of the Scaglia Rossa Formation is due to rhythmic alternation of thin (usually <20 cm thick) limestone beds and thin (a few mm) shale partings. Limestone beds mostly consist of calcareous nannofossils with ~5% aeolian clay (Lowrie et al., 1990). The limestone beds have stylolites and calcite veins that indicate partial calcite dissolution, but undisturbed fossils suggest that pervasive recrystallization has not occurred (Arthur and Fisher, 1977). Shale partings have lower carbonate contents (>60% on average, e.g., Rocchia et al., 1990), and higher concentrations of terrigenous (aeolian) clay and silt (Arthur and Fisher, 1977). Formation of bedding in carbonate sequences is generally not well understood. By analogy with siliciclastic sequences, rhythmic alternation of limestone and shale is conventionally interpreted as reflecting variations in carbonate productivity due to changes in the amount of incoming solar radiation caused by variation of the Earth's orbit. Recent studies, however, suggest that limestone and shale layers may form in carbonate successions as a result of differential diagenesis involving complex carbonate dissolution–reprecipitation processes, differential compaction, and passive enrichment–dissolution of inert non-carbonate components (e.g., Bathurst, 1972; Ricken, 1986; Westphal, 2006; Westphal et al., 2010).

Arthur and Fisher (1977) presented clear evidence that the Scaglia Rossa Formation has been affected by differential diagenesis. They observed systematic trends in detrital elements (Fe, Ti, Si, Al) across bedding couplets, with maximum concentrations

in shale interbeds and progressive decreases toward the centre of limestone beds. While bulk chemical and magnetic characteristics of the limestone and shale interbeds are similar on a carbonate-free basis (e.g., Rocchia et al., 1990), which is consistent with a simple carbonate dilution model, detailed clay mineral results reveal qualitative and quantitative differences between the mineralogical compositions of the shales and limestones, which is indicative of a change in clastic source(s) during deposition (Johnsson and Reynolds, 1986). To test for possible systematic magnetic differences between limestone and shale interbeds that might bear on climatic interpretation of the K–Pg interval, we analyzed limestone beds 70 cm below to 70 cm above the K–Pg boundary (defined at the base of the boundary clay; Molina et al., 2006) and 8 shale interbed samples.

2.2. Bidart section

The well-studied Bidart section is located in southwestern France, along Erreteguia beach about 2 km north of Bidart village (Fig. 1). The section is composed of Maastrichtian gray to red-brown marls and marly limestones and Danian white to pinkish white massive limestone. The K–Pg transition is characterized by distinct lithological changes. The Maastrichtian marls change color to yellowish-gray ~30 cm below the K–Pg boundary (Fig. 1). The boundary is marked by a 15-cm-thick clay layer with increased Ir concentration at the base (Bonté et al., 1984). The clay horizon is overlain by red marly limestones, followed by massive white limestones. The clay contact with the underlying Maastrichtian beds is relatively sharp, while a gradual transition occurs into the overlying Danian limestones.

Paleomagnetic and rock magnetic characteristics of the K–Pg interval of the Bidart section have been presented by Galbrun and Gardin (2004) and Font et al. (2011). To ensure consistent assessment of the K–Pg transition between the two studied sections, we selected sixteen representative samples from the Bidart sequence (that can be correlated directly to the study of Font et al., 2011) for detailed magnetic characterization using the same equipment and measurement protocol as for samples from the Gubbio section.

3. Methods

Limestone samples from Gubbio were cut into ~1-cm-thick subsamples in stratigraphic order. The cut samples were analyzed with a vibrating sample magnetometer (VSM) to measure hysteresis parameters, isothermal remanent magnetization (IRM) acquisition curves and first-order reversal curves (FORCs). Samples from shale interbeds and crushed samples from the Bidart section were ground with an agate mortar and were packed into gelatine capsules for measurements. In addition, 50–100 mg of ground material from representative samples was used for low-temperature magnetic measurements with a Quantum Design Magnetic Properties Measurement System (MPMS). For limestone beds from Gubbio, low-temperature measurements were made on samples from the middle part of the beds.

Magnetic measurements were made at the Australian National University (ANU), Canberra, Australia. For all samples, hysteresis loops were measured from +1 to −1 T with a Princeton Measurements Corporation MicroMag Model 2900 VSM. Saturation magnetization (M_s), saturation remanent magnetization (M_r), and coercive force (B_c) were obtained from hysteresis loops after subtracting the paramagnetic contribution. The coercivity of remanence (B_{cr}) was obtained by demagnetizing M_r in a stepwise increasing back-field. Coercivity spectra were evaluated from IRM acquisition curves (Robertson and France, 1994) that were measured with 70 logarithmically scaled steps, up to a maximum peak field of 1 T. IRM acquisition curves were decomposed into coercivity components using the fitting program of Kruiver et al. (2001), which is limited to symmetric distributions in logspace. Magnetic components are characterized by the saturation IRM (SIRM), which is proportional to the magnetic mineral concentration in a sample, the peak field at which half of the SIRM is reached ($B_{1/2}$), and the dispersion parameter (DP) for the corresponding cumulative lognormal distribution (Kruiver et al., 2001). The maximum available field on the VSM (1 T) is insufficient for reliable characterization of high-coercivity minerals such as hematite and goethite, so IRM acquisition curves were measured for 12 representative samples using a MPMS (with 26 logarithmically scaled steps, up to 7 T). IRM components for hematite and goethite determined from the MPMS measurements were then used to fit the high-coercivity part of IRM acquisition curves measured on the VSM.

High-resolution FORC measurements (Pike et al., 1999; Roberts et al., 2000, 2014) were made for representative samples (one sample per limestone bed and one per shale layer) with the VSM. To improve the signal-to-noise ratio of FORC measurements, samples were measured multiple times (2–12 repetitions) and the FORC distributions were averaged. FORCs were measured with a saturating field of 0.5 T, an averaging time of 200 ms and a wait time of 1 s between successive measurements, and were processed using the algorithm of Heslop and Roberts (2012). For representative limestone-shale couplets, each measurement run included 300 FORCs measured with a field increment of 0.495 mT, and were processed with a smoothing factor (SF) of 5. For the remaining samples, each measurement run included 230 FORCs measured with a field increment of 0.633 mT; FORCs were processed using an optimal SF of 3. These SF and field increment values provide optimal resolution of the central ridge feature that is indicative of intact magnetofossil chains (Egli et al., 2010).

Characteristic low-temperature magnetic behavior of iron oxides, such as the magnetic phase transition in magnetite (the Verwey transition) and enhanced remanence on cooling that is typical of goethite (Dekkers, 1989; Liu et al., 2006), was monitored with the MPMS. For low-temperature measurements, an IRM was imparted at room temperature (300 K) in a 7 T field; the remanence was then measured in zero-field during cooling from 300 to 10 K, followed by warming from 10 to 400 K and subsequent cooling back to 300 K.

4. Results

4.1. Hysteresis parameters

Hysteresis loops for Gubbio limestone samples (Fig. 2) are wide with a clear constriction in the middle that is indicative of distinct ferrimagnetic mineral populations with strongly contrasting coercivities (Roberts et al., 1995; Tauxe et al., 1996). There is a distinct difference in hysteresis loop shape for background Cretaceous and Paleogene samples. Compared to Paleogene samples, Cretaceous samples have wider loops with higher coercivity and M_r/M_s values (indicative of a higher contribution from high coercivity minerals). M_s depends on magnetic mineral concentration, which has values that are on average about twice as high in Paleogene samples compared to background Cretaceous samples. Hysteresis loops for limestone samples from the LSZ at Gubbio have about an order of magnitude lower M_s values compared to background Cretaceous sediments, but have a generally similar appearance, albeit with smaller loop constriction (signifying a smaller relative low coercivity contribution). Hysteresis loops for shale interbeds generally have similar shapes to those of adjacent limestone beds, with minor increases in B_{cr} and M_r/M_s

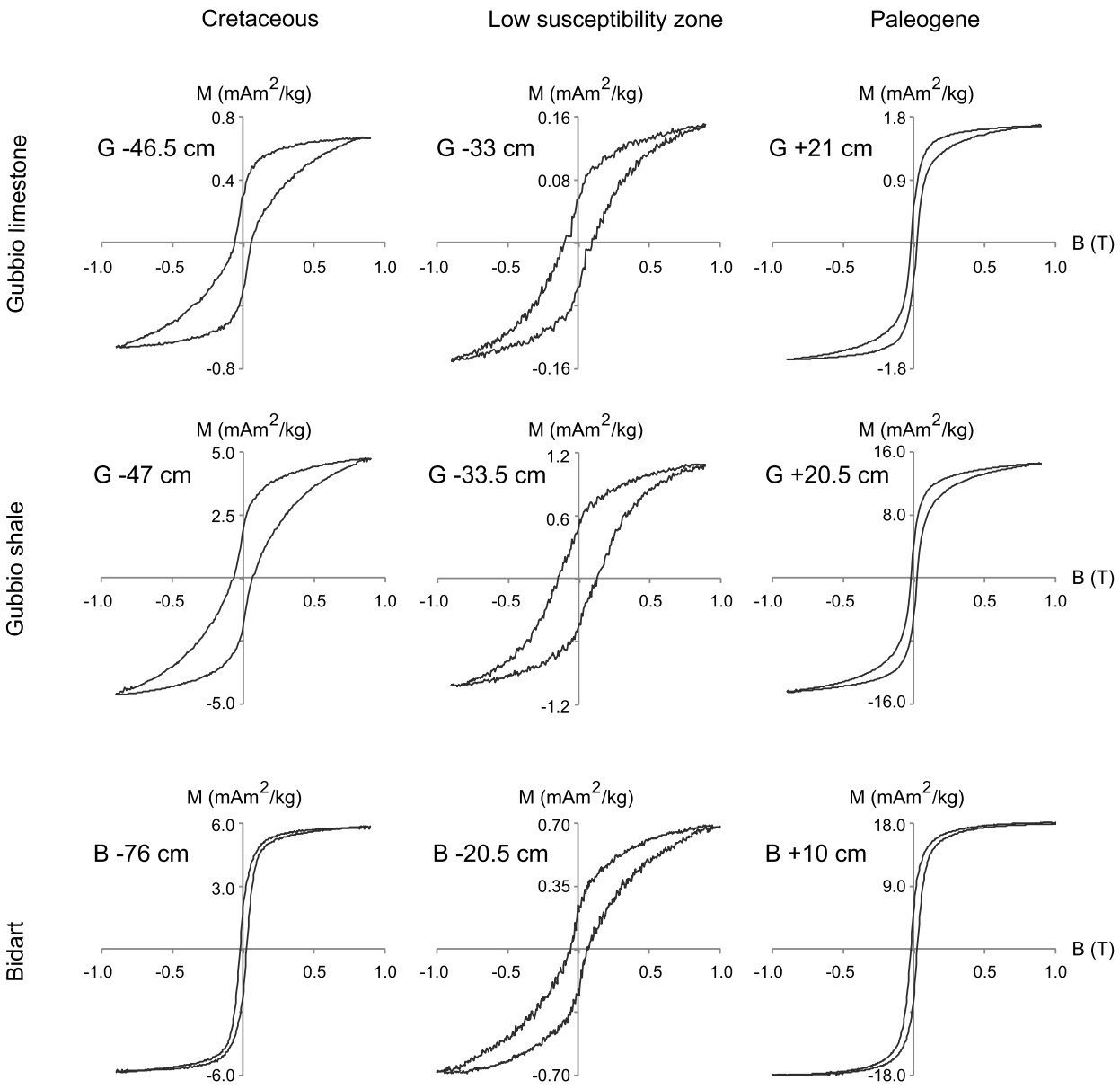

Fig. 2. Representative examples of hysteresis loops (after paramagnetic correction) for background Cretaceous (Maastrichtian) sediments, the low susceptibility zone, and Paleogene (Danian) samples from the Gubbio and Bidart sections. For Gubbio, hysteresis loops from limestone and adjacent shale interbeds are shown for comparison. The number in the sample labels denotes the stratigraphic position with respect to the K–Pg boundary (base of the boundary clay layer).

values that indicate a small decrease in the relative contribution from low coercivity magnetic minerals, but with approximately ten times higher values of concentration-dependent parameters, M_s and M_r.

Hysteresis loops for background Cretaceous and Paleogene samples from the Bidart section have consistently "normal" shapes, with no evidence of wasp-waisted or pot-bellied forms (Tauxe et al., 1996). This loop shape indicates a predominance of low coercivity magnetic minerals in the Bidart marls. The loops, however, do not close completely at 0.6 T, which suggests the presence of high coercivity minerals. Compared to the rest of the section, samples from the LSZ at Bidart have up to an order of magnitude lower M_s values, as well as distinctly different overall hysteresis loop shapes. LSZ samples have higher saturation field (>0.95 T) and coercivity values, and a distinct wasp-waisted constriction of loops. These features indicate the predominance of high coercivity minerals in the LSZ, with only a minor contribution from low coercivity minerals.

4.2. IRM acquisition

Representative IRM acquisition curves for the studied intervals are shown as gradient plots in Fig. 3. Up to five distinctive magnetic components with variable contributions to the total IRM can be identified by statistical analysis (Kruiver et al., 2001). The lowest coercivity component with mean coercivity $B_{1/2}$ of ~20–40 mT and a wide DP of 0.35–0.45 is present in all samples. The coercivity range of this component is typical of titanomagnetite and maghemite and their mixtures, while the wide dispersion is characteristic of a detrital source (e.g., Kruiver et al., 2001; Egli, 2004). Detrital iron oxides (magnetite and ilmenite) have been identified in the studied rocks from Bidart with SEM observations and EDS analyses (Font et al., 2011, 2014). Although this magnetic mineral population may also include particles that formed by inorganic precipitation (Maher, 1988), or by dissimilatory iron-reducing bacteria (Moskowitz et al., 1989), for simplicity this component is referred to as "detrital magnetite" in the following discussion.

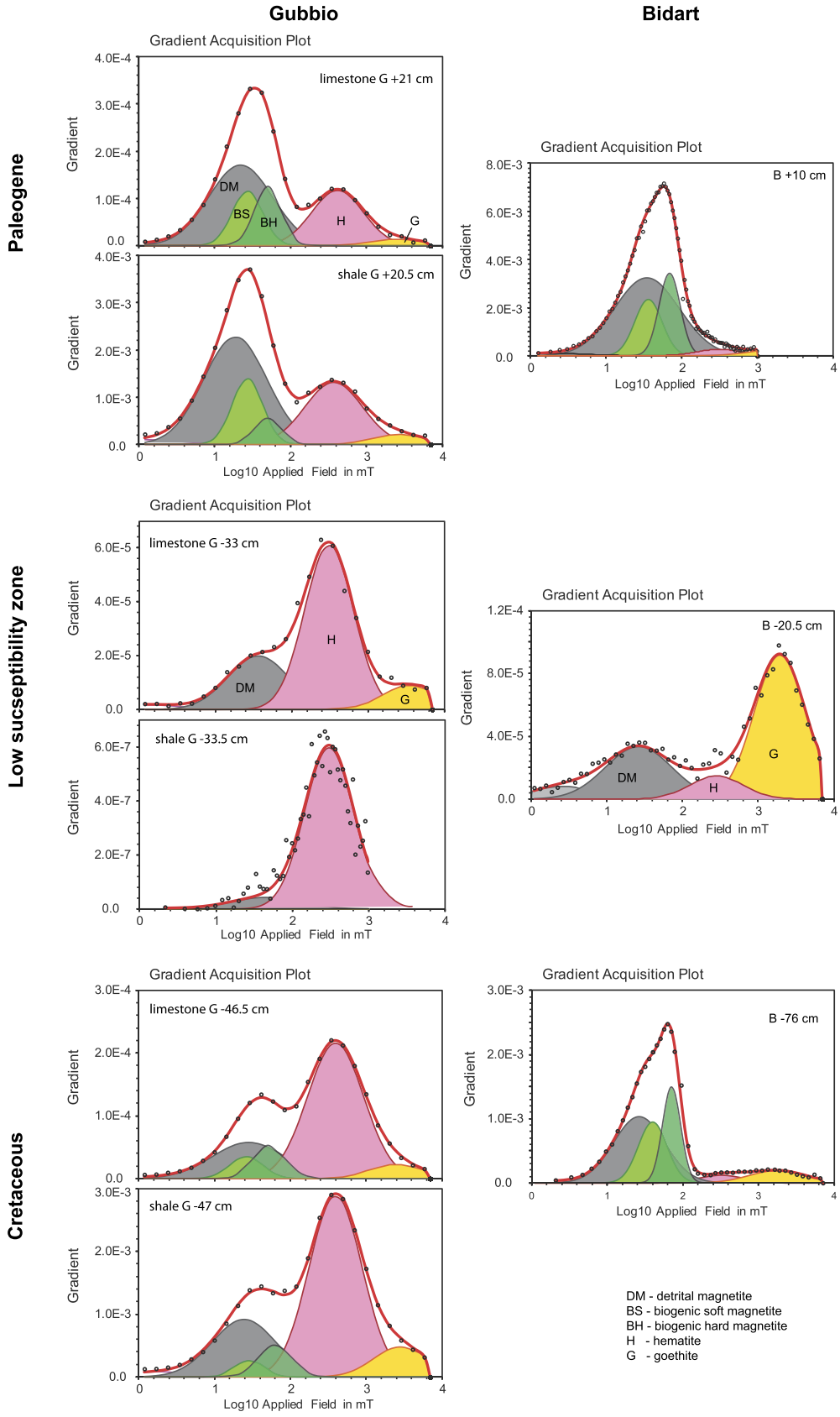

Fig. 3. IRM (gradient) acquisition curves for representative samples of background Cretaceous (Maastrichtian) sediments, the low susceptibility zone, and Paleogene (Danian) samples from the Gubbio and Bidart sections. For Gubbio, IRM acquisition curves for limestone and adjacent shale interbeds are shown for comparison. Up to five magnetic components with variable contributions to the total IRM are identified by statistical analysis (Kruiver et al., 2001). Based on characteristic coercivities and DP values, the components are: detrital magnetite/maghemite (DM), biogenic soft (BS) and biogenic hard (BH) magnetite, hematite (H), and goethite (G).

Two other components in the low coercivity range with $B_{1/2}$ of ~26–70 mT are characterized by a narrow DP of 0.12–0.20, which is indicative of uniform grain sizes and/or composition of the magnetic particle population. Such uniform assemblages are typical of magnetic particles (magnetosomes) produced by magnetotactic bacteria (e.g., Kruiver and Passier, 2001; Egli, 2004). Two biogenic components, biogenic soft (BS) and biogenic hard (BH), are commonly observed in recent (e.g., Egli, 2004; Yamazaki, 2012) and ancient (e.g., Abrajevitch et al., 2011; Roberts et al., 2013; Heslop et al., 2014) sediments. The difference in median coercivity of the two populations is usually attributed to differences in magnetosome morphology (e.g., Egli, 2004; Yamazaki, 2012; Heslop et al., 2014), or to their preservation mode, e.g., intact vs. collapsed magnetosome chains (e.g., Kobayashi et al., 2006).

An intermediate coercivity component ($B_{1/2}$ ~ 250–450 mT; DP ~ 0.27–0.45), and a high-coercivity component ($B_{1/2}$ ~ 1.6–2.5 T; DP ~ 0.3–0.35) are identifiable in all IRM acquisition curves with a maximum applied field of 7 T. Based on their characteristic coercivities, the intermediate- and high-coercivity components can be identified as hematite and goethite, respectively (e.g., Heller, 1978; France and Oldfield, 2000; Kruiver et al., 2001; Abrajevitch et al., 2009). The continuing remanence increase up to the maximum applied field of 1 T suggests the presence of goethite, although its contribution is difficult to quantify with confidence because it is not magnetically saturated at this field. To estimate the hematite concentration, the contribution of goethite to the high coercivity part of the 1-T IRM spectra was estimated using the mean coercivity and DP of the goethite component from fitting of the 7-T IRM curves.

For the Gubbio samples, the overall shape of IRM acquisition curves for limestones and adjacent shale interbeds is similar; the major difference is in concentration-dependent SIRM values (note the order-of-magnitude difference in gradient scale between limestone and shale in Fig. 3). The curve fitting reveals variations in relative contributions from BH and BS components between limestone and adjacent shale interbeds (Fig. 3). Danian samples from Gubbio have consistently higher relative contributions from low coercivity components compared to Maastrichtian sediments. The relative contribution of detrital magnetite versus hematite components from the LSZ at Gubbio resembles background Maastrichtian sediments. However, LSZ samples are distinct in their lack of biogenic components.

For the Bidart samples, IRM acquisition curves are dominated by low coercivity components. Fitting of the 7-T curves also reveals a substantial goethite component. In samples from the LSZ, goethite contributes dominantly to the IRM. Similar to Gubbio, samples from the Bidart LSZ also lack biogenic peaks.

4.3. FORC diagrams

High-resolution FORC diagrams for representative samples from Gubbio and Bidart are shown in Fig. 4. In background Maastrichtian and Danian sediments, FORC diagrams for samples from both sections have a characteristically narrow “central ridge” signature with a wide maximum along the B_c axis and a narrow distribution along the B_u axis (Fig. 4). The narrow ridge is indicative of non-interacting single-domain particles (Roberts et al., 2000; Egli et al., 2010) that is characteristic of fossil magnetosomes (Egli et al., 2010; Li et al., 2010; Roberts et al., 2013; Heslop et al., 2014). There is a systematic difference in central ridge coercivity profiles for limestone and adjacent shale interbeds at Gubbio, with a higher median coercivity in limestone samples. Such variations are suggestive of different structures of magnetofossil assemblages, with a higher BH content in limestone samples. For the Bidart samples, the central ridge has a wider B_c range and higher median coercivity compared to those from Gubbio. The characteristic central ridge signature is absent in FORC diagrams from the LSZ interval at both sections (Fig. 4).

4.4. Low temperature measurements

The low-temperature magnetic behavior of the studied samples varies significantly (Fig. 5). In the Danian and Maastrichtian samples from Gubbio, the Verwey transition of magnetite is detected as a stepwise drop in magnetization at ~120 K (Fig. 5a, c). In adjacent shale samples and in LSZ limestone samples, the suppressed Verwey transition is indicated by separation of the cooling and warming curves (Fig. 5b, e). For the Gubbio samples, an IRM acquired at room temperature (RT IRM) initially rises on cooling, but the increase is not large (<30% of the initial RT IRM). On heating from 300 to 400 K, a kink in the slope of the warming curve is observed at ~360 K in some samples (e.g., Fig. 5c, e, f), while the remanence loss is gradual in others (Fig. 5a, d). The remanence loss on heating is not recovered on cooling back to 300 K. The irreversible remanence loss on warming through ~360 K (the Néel temperature) is typical of goethite (e.g., Carter-Stiglitz et al., 2006; Liu et al., 2006). The contribution of goethite to the IRM can be estimated as the remanence loss in the 300 K ⇒ 400 K ⇒ 300 K cycle after Carter-Stiglitz et al. (2006) (e.g., Fig. 5d), although some fraction of the IRM loss can be due to superparamagnetic (SP) hematite and magnetite.

In contrast to the Gubbio samples, the low temperature behavior of the Bidart samples is characterized by a significant, up to 300%, increase in RT IRM on cooling to 10 K (Fig. 5g, j, h, i). The magnetization increase is essentially reversible, with the IRM recovering its intensity on the return to 300 K. A kink at ~360 K and a non-recoverable IRM loss are observed in the warming-cooling cycles. The large reversible IRM increase on cooling accompanied by non-recoverable remanence loss on warming indicates a significant contribution from goethite (e.g., Carter-Stiglitz et al., 2006; Liu et al., 2006). In complementary measurements, when RT IRM was heated to 400 K prior to the cooling cycle in order to thermally demagnetize goethite, the Verwey transition of magnetite is observed either as a stepwise IRM drop (e.g., Fig. 5l), or, more often, as a separation of cooling and warming curves at ~100 K (Fig. 5j, k).

With a possible exception of sample G-46.5 cm (Fig. 5c), in which a change in slope at 250 K may indicate a suppressed Morin transition (Morin, 1950) due to hematite, no other samples have a clear expression of this transition. The absence of a Morin transition in samples that contain hematite (as identified by its typical IRM acquisition characteristics) is typical of marine sediments (e.g., Abrajevitch et al., 2009, 2013; Abrajevitch and Kodama, 2011) and is indicative of small (>30 nm) hematite particle sizes (Özdemir et al., 2008).

5. Discussion

5.1. Formation of limestone-shale couplets at the Gubbio section

Comparison of the magnetic properties of limestone beds with those of adjacent shale interbeds indicates systematic differences between the two lithologies (Fig. 6). Apart from about an order of magnitude difference in bulk concentration of ferrimagnetic phases, as indicated by concentration-dependent hysteresis parameters M_s and M_r (Fig. 2) and SIRM values (Fig. 3), there are also systematic differences in concentration-independent parameters, e.g., M_r/M_s, that are indicative of differences in median grain-size or composition of ferrimagnetic mineral assemblages (e.g., Dekkers, 2007). Limestone beds not only have higher relative abundances of biogenic (BS + BH) grains (Fig. 6), but also

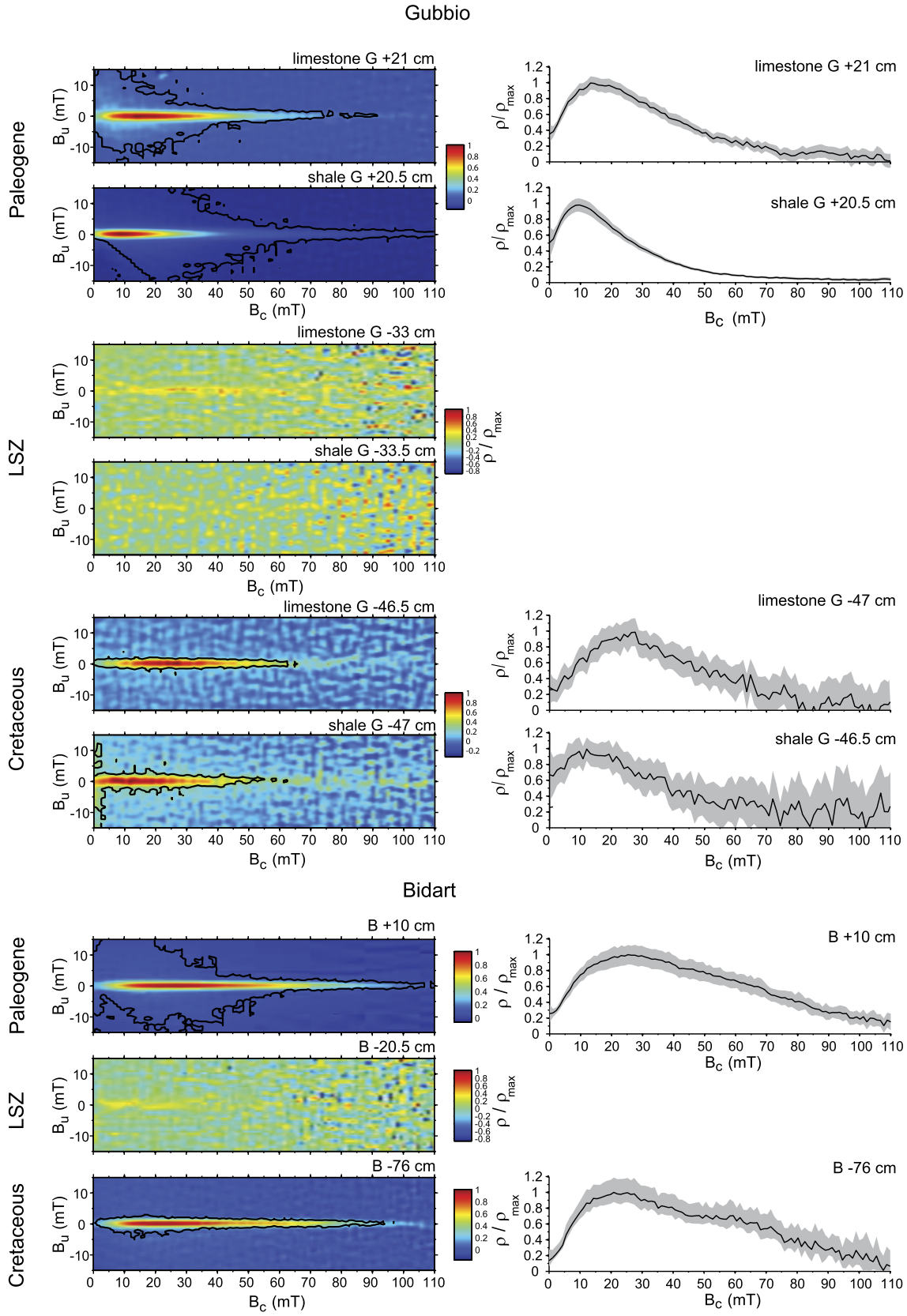

Fig. 4. High-resolution FORC diagrams for representative samples from background Cretaceous (Maastrichtian) sediments, the low susceptibility zone, and Paleogene (Danian) samples from the Gubbio and Bidart sections. A narrow peak along the B_u axis, which is typical of fossil magnetosomes (Egli et al., 2010), is present in background Maastrichtian and Danian sediments, but is absent in samples from the low susceptibility zone at both sections. FORC diagrams are plotted using the algorithm of Heslop and Roberts (2012) with SF = 5 for the Gubbio samples, and SF = 3 for the Bidart samples. The black contour denotes the 0.05 significance level. The gray shading on the profiles on the right-hand side indicates the 95% confidence interval around the mean ρ/ρ_{max} value (black line).

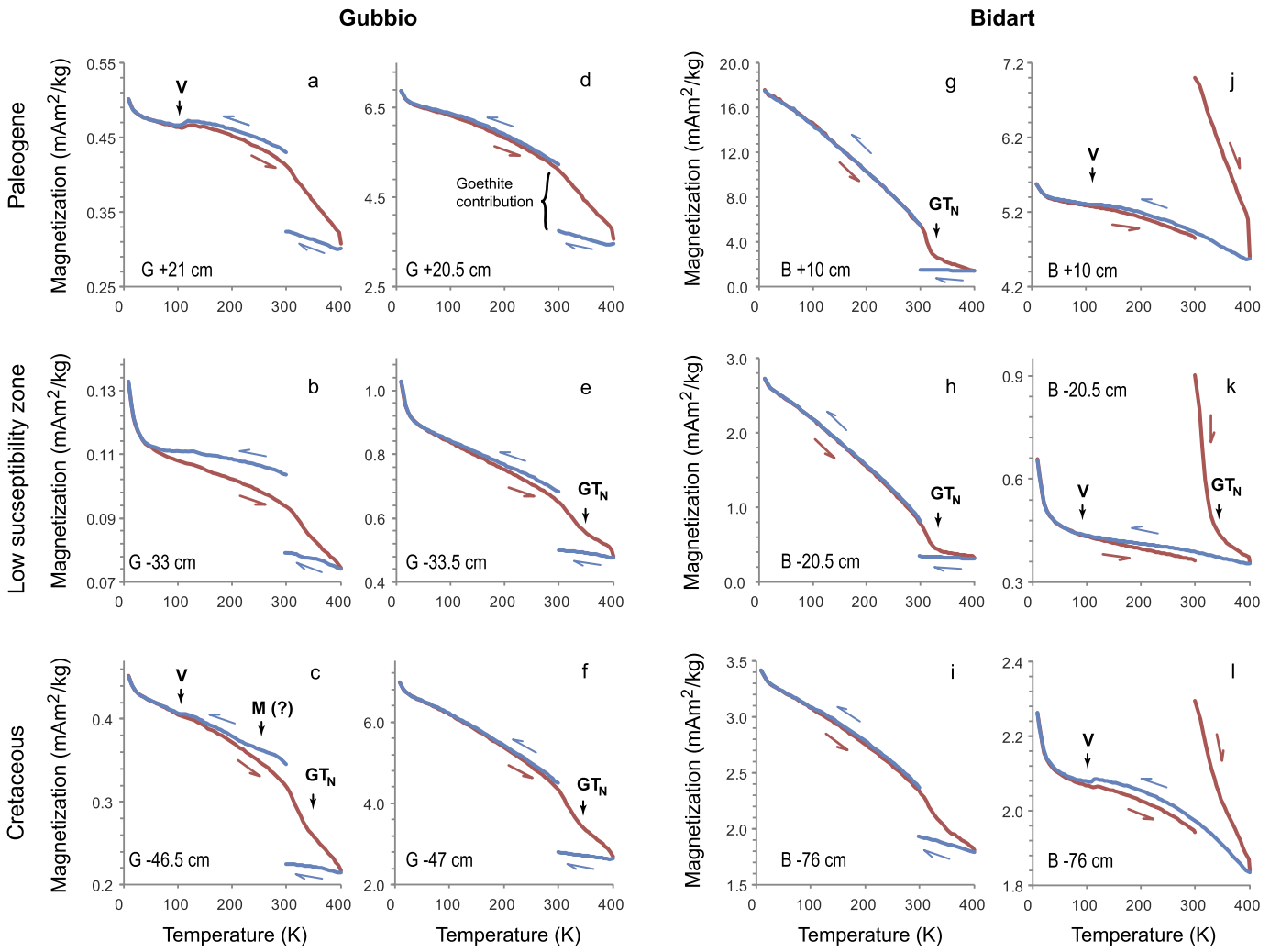

Fig. 5. Temperature dependence of an isothermal remanent magnetization acquired at room temperature (300 K) in a 7-T field (RT IRM) for representative samples from (a, d, g, j) Paleogene (Danian), (c, f, i, l) background Cretaceous (Maastrichtian), and low susceptibility zone (b, e h, k) sediments from the (a–f) Gubbio and (g–l) Bidart sections. Arrows indicate characteristic low temperature features, such as the Verwey transition for magnetite (V), the Morin transition for hematite (M), and the Néel temperature for goethite (GT_N). For Gubbio limestone and shale samples (columns 1 and 2), the temperature cycle includes cooling from 300 K to 10 K, followed by warming from 10 K to 400 K, then by cooling back to 300 K. During the same temperature cycle, the low temperature behavior of Bidart samples (column 3) is dominated by a significant IRM increase on cooling that is typical of goethite. Such large remanence changes mask other characteristic low temperature features. For these samples, supplementary measurements include temperature cycling from room temperature (300 K) to 400 K (to thermally demagnetize goethite), then cooling from 400 K to 10 K, and warming back to 300 K (column 4). Supplementary cycles reveal the Verwey transition in the Bidart samples.

differ from shale interbeds in the structure of magnetofossil assemblages; high-resolution FORC diagrams have higher median coercivity (a higher proportion of BH grains) in limestones (Fig. 4). These systematic differences are inconsistent with the simple carbonate dilution model of limestone-shale formation. The dissimilar biogenic features suggest that environmental/authigenic conditions were different during periods of high productivity (high carbonate flux) and low productivity. The close association of magnetofossil assemblages with lithology, which is also seen in bedded siliceous sequences (Abrajevitch et al., 2011), indicates that biogenic magnetizations in bedded marine sequences were acquired contemporaneously with deposition.

Previous investigations of the K–Pg interval at Gubbio have often focused on comparing characteristic features of the boundary clay layer to those of adjacent limestone beds (e.g., Lowrie et al., 1990; Verma et al., 2002). Such comparisons may not be justifiable because the difference between these lithologies may be at least partially due to diagenetic variations, rather than reflecting a unique impact-related change. To ensure that our evaluation is not biased by differential diagenesis, we focus on limestone beds only in the following discussion.

5.2. Magnetic mineral variations

Concentration-dependent magnetic measurements are shown across the K–Pg interval for the Gubbio and Bidart sections in Fig. 7. Variations in the amount of detrital magnetite, biogenic magnetite (sum of the BH and BS components), and hematite are approximated by SIRM parameters determined from IRM acquisition curves up to 1 T. Goethite contributions were estimated following Carter-Stiglitz et al. (2006) as the loss of RT IRM (acquired in a 7 T field) on heating from 300 K to 400 K and cooling back to 300 K.

Compared to background Cretaceous sediments, the bulk ferrimagnetic mineral content in the LSZs is significantly lower (Fig. 7). At Gubbio, detrital magnetite, hematite and goethite concentrations decrease by at least an order of magnitude in the LSZ, similar to the findings of Lowrie et al. (1990). At Bidart, however, the significant decrease in detrital magnetite concentration is not ac-

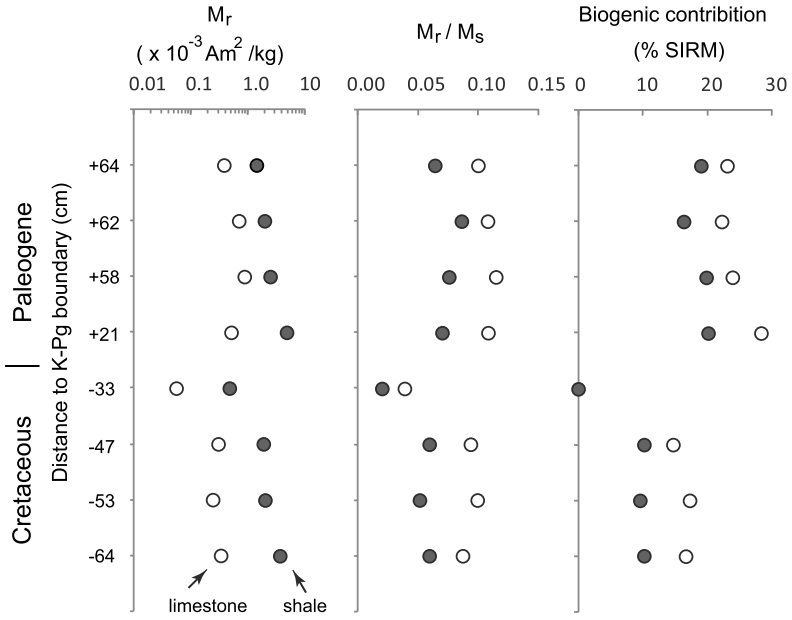

Fig. 6. Rock magnetic characteristics of representative limestone-shale couplets from the Gubbio sequence.

companied by a concomitant decrease in hematite and goethite contents. Disappearance of the biogenic component in the LSZ, as indicated by IRM acquisition (Fig. 3) and FORC measurements (Fig. 4), is common to both sections.

Relative abundances of magnetic phases in marine sediments can be used to evaluate climatic and diagenetic conditions during sedimentation. Relative abundances of hematite and goethite in marine sediments, for example, are often used to estimate precipitation regimes in the source area of detrital sediments, with higher moisture availability promoting formation of goethite over hematite (e.g., Harris and Mix, 1999; Zhang et al., 2007). However, hematite is significantly more stable than goethite to reductive dissolution (e.g., Poulton et al., 2004; Abrajevitch et al., 2009; Abrajevitch and Kodama, 2011). The initial ratio of these detrital minerals is, therefore, often modified during marine early diagenesis.

Based on its delayed remanence acquisition, hematite in the Gubbio and Bidart sequences is thought to have an authigenic origin, with formation via nucleation and gradual growth through the critical single-domain threshold volume (Channell et al., 1982; Galbrun and Gardin, 2004). A strong correlation between hematite content and that of other terrigenous indicators, e.g., clay content in limestone-shale couplets at Gubbio and other bedded sequences (e.g., Abrajevitch et al., 2011), suggests two things; first, that iron for chemical reactions culminating in formation of hematite pigment was introduced with the detrital mineral assemblage, and second, that vertical diffusive redistribution of iron during diagenesis was insignificant.

Iron-bearing precursors to hematite would have arrived with the aeolian (e.g., Arthur and Fisher, 1977) sediment component and are likely to have been composed of highly reactive iron oxyhydroxides that commonly constitute a considerable portion of aeolian dust (Baker et al., 2006; Fan et al., 2006). Such iron oxyhydroxides are unstable during early diagenesis (e.g., Poulton et al., 2004). Iron released during reductive dissolution of oxyhydroxides may diffuse out of sediments into the overlying water column, to be partially consumed by biota and/or re-deposited elsewhere, or may be incorporated into neo-formed authigenic minerals, such as hematite, goethite or iron sulphides. Unstable early diagenetic phases may undergo further alteration during oxic diagenesis that follows the initial reductive phase, with formation of hematite as the final alteration product. Regardless of whether authigenic hematite was formed by direct precipitation from solution, or through alteration of oxidized or reduced intermediate phases, the hematite content of the sediment is ultimately controlled by the amount of available iron. Thus, the hematite content of the sediments is indirectly (through the amount of reactive iron) indicative of the initial detrital sediment composition.

While magnetite and hematite formation in the studied sections can be constrained to have been approximately syndepositional based on paleomagnetic data (Channell et al., 1982; Galbrun and Gardin, 2004), the source and timing of goethite formation is less certain. In marine sediments, goethite can have a detrital origin (e.g., van der Zee et al., 2003). Goethite forms commonly in acidic solutions, where hematite precipitation is retarded (Schwertmann and Murad, 1983). Goethite is also a common product of iron mineral alteration in surface environments, particularly in soils developed on carbonate-rich substrates (e.g., Cornell and Schwertmann, 2006). High concentrations of goethite in the boundary clay have been reported from other well-studied K–Pg boundary sections, where its formation has been explained as resulting from early diagenesis under anomalous post-impact conditions (e.g., Pechersky, 2008; Osete et al., 2010). The Bidart sequence has a similar relative goethite increase at around the K–Pg boundary level; at Gubbio, however, no goethite enrichment is observed. Thus, goethite enrichment at the K–Pg boundary probably does not reflect a global environmental signal, but is rather due to local conditions; either in the aftermath of the impact, or during later weathering of iron silicates from the boundary clay.

A significant decrease in detrital magnetite content accompanied by the disappearance of biogenic magnetite (Figs. 3, 7) is observed in the LSZs at both Gubbio and Bidart. As mentioned above (Section 4.2), the “detrital” magnetite component may include a fraction of authigenic, extracellular biogenic or abiogenic magnetite particles, or disjointed magnetite particles from collapsed magnetosome chains. Such particles tend to have similar size and stoichiometry as detrital magnetite grains, as evidenced by indistinguishable IRM acquisition parameters (e.g., Egli, 2004). While detrital and authigenic particles may differ somewhat in their surface reactivity, which ultimately controls dissolution rates (e.g., some detrital grains may be partially protected by occurring within silicate host minerals), these potential variations are consid-

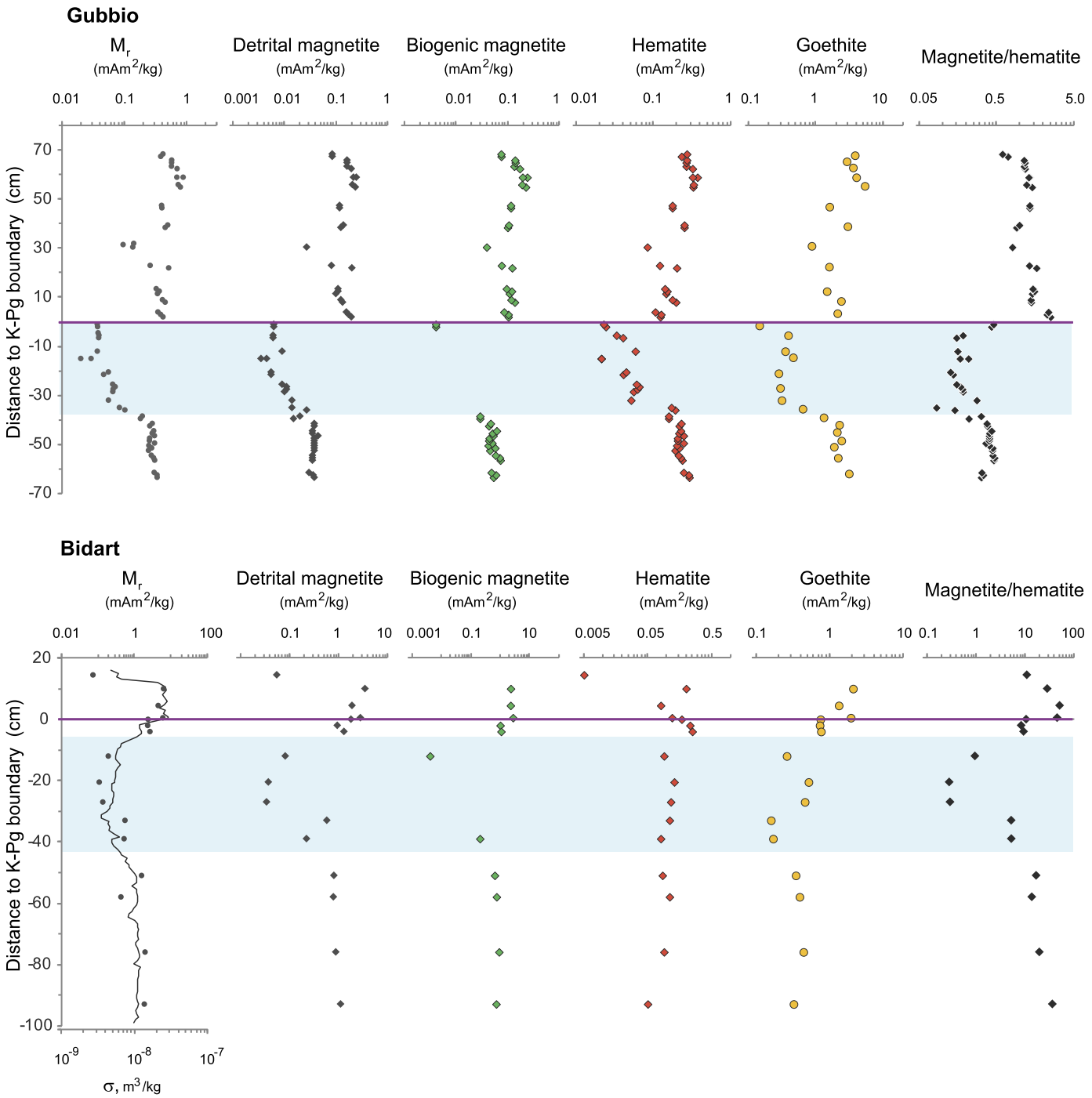

Fig. 7. Variations in the saturation remanence (M_r), detrital and biogenic magnetite, hematite, and goethite contents, and the relative abundance of magnetite and hematite across the Cretaceous–Paleogene boundary at the Gubbio (upper) and Bidart (lower) sections, respectively. The bulk ferrimagnetic mineral content is approximated by M_r values from hysteresis loops (maximum applied field of 1 T) and, for the Bidart section by mass-specific susceptibility data from Font et al. (2011). Detrital and biogenic magnetite and hematite contents were estimated from IRM component analysis (Kruiver et al., 2001). Goethite content is evaluated from low temperature cycling (from the IRM loss on warming from 300 K to 400 K and then cooling back to 300 K after the low temperature run (300 K ⇒ 10 K ⇒ 300 K), following Carter-Stiglitz et al., 2006). The logarithmic scale in this figure is used because of large variations in ferrimagnetic mineral concentration between the Cretaceous and Paleogene intervals at Gubbio, to highlight the critical feature – the decreased magnetic mineral concentration at the end of the Cretaceous.

ered to be insignificant for our interpretation. An overall decrease in concentration of the "detrital" component is indicative of a decreased magnetite concentration.

As the stability of magnetite to reductive dissolution is lower than that of hematite (e.g., Poulton et al., 2004; Abrajevitch et al., 2009; Abrajevitch and Kodama, 2011), diagenetic dissolution in marine environments often leads to decreased relative abundances of magnetite and hematite, which we observe in the LSZ at both sections (Fig. 7). Dissolution rates depend on interfacial surface area, therefore, smaller ferrimagnetic grains, with higher surface area to volume ratio, dissolve more rapidly. Biogenic magnetite, because of its uniformly small size, is particularly sensitive to diagenetic dissolution and oxidation that may result in loss of characteristic magnetic fingerprints (e.g., Abrajevitch and Kodama, 2011; Chang et al., 2013). Alternatively, disappearance of a biogenic signature in the studied sections may reflect a local extinction of

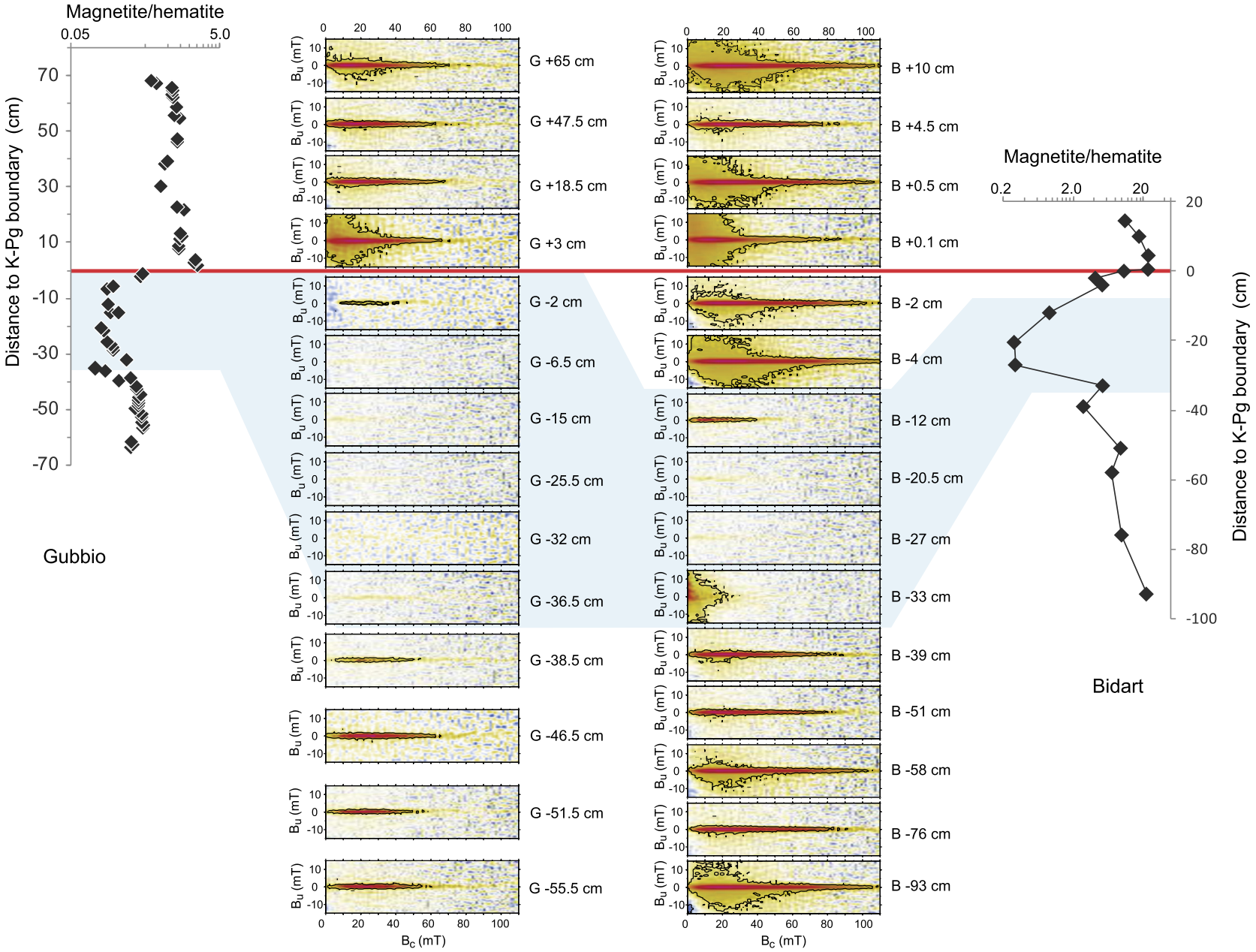

Fig. 8. FORC characteristics of the K–Pg transition intervals at Gubbio and Bidart. The sharp central ridge that dominates FORC diagrams for background Maastrichtian and Danian sediments at Gubbio and Bidart is indicative of non-interacting SD particles that reflect the presence of magnetite magnetofossils (Egli et al., 2010). The combination of a sharp central ridge and large vertical spread (e.g., *B* +10 cm and *B* −93 cm) indicates a mixed magnetic mineral assemblage with SD biogenic magnetite and coarser PSD/MD detrital particles. The central ridge is absent in samples from the low susceptibility zones at both sections. However, the statistically significant central ridge is present in samples from below the K–Pg boundary, in one sample at Gubbio (*G* −2 cm), and in samples from the −2 cm to −12 cm interval at Bidart. FORC diagrams were calculated using the algorithm of Heslop and Roberts (2012); the black line on the FORC diagrams represents the 0.05 significance level.

magnetotactic bacteria, or a decrease in their abundance to numbers below the detection limit of the methods used in this study. Although the physiological requirements of magnetotactic bacteria are poorly known, changing local nitrogen and oxygen contents (e.g., Frankel et al., 1997; Salazar et al., 2011), ambient temperature (Lefèvre et al., 2010; Lin et al., 2012), pH and alkalinity (Lefèvre et al., 2011; Abrajevitch et al., 2013), and nutrient availability (e.g., Roberts et al., 2011; Liu et al., 2015) have all been argued to be important factors for magnetotactic bacteria. Regardless of the exact mechanism, the absence of magnetofossils within the LSZ indicates a temporal environmental perturbation when conditions became unfavorable either for magnetotactic bacterial growth or for magnetofossil preservation.

Decreased detrital magnetite and hematite concentrations, with a larger relative loss of magnetite, accompanied by disappearance of biogenic magnetite (Fig. 7), are generally consistent with the reductive dissolution model of Lowrie et al. (1990) for LSZ formation at Gubbio. Syndepositional formation of hematite pigment at Gubbio and Bidart inferred from paleomagnetic studies (Channell et al., 1982; Galbrun and Gardin, 2004), however, is incompatible with this explanation. Reducing conditions during diagenesis are not conducive to hematite formation, which, instead, requires oxic conditions (e.g., Cornell and Schwertmann, 2006). More likely, then, is that the observed variations in relative magnetite and hematite abundance reflect a change in detrital source compositions within the LSZ, as discussed in more detail below in Section 5.4.

5.3. Biogenic magnetite in the K–Pg interval

FORC diagrams for the studied sediments (Fig. 8) provide further clues about LSZ formation. Although the exact cause, through either extinction of bacteria versus diagenetic dissolution of magnetofossils, cannot be confidently determined to explain the disappearance of biogenic magnetite, variations in biogenic magnetite characteristics and abundances provide a useful indicator of environmental change. The presence of a central ridge signature (Egli et al., 2010) in all background Maastrichtian and Danian sediments from both sections indicates that magnetofossil burial is an intrinsic part of the normal sedimentation process. The central ridge disappears in the LSZ at both sections where detrital magnetite contents are lowest. At the base of the Bidart LSZ, instead of a central ridge, a strong low coercivity peak is centered at the origin of the FORC diagram (Fig. 8, B −33 cm), which is characteristic of SP grains (Pike et al., 2001). A similar increase in the SP fraction occurs at the base of a reductive dissolution zone in Australian continental margin sediments, where SP grains are interpreted to have formed by partial dissolution of single-domain magnetosomes (Abrajevitch and Kodama, 2011).

Above the LSZ, the FORC central ridge signature re-appears below the boundary clay layer. At Gubbio, the limestone bed that lies immediately below the boundary clay has a weak, but statistically significant, central ridge signature (Fig. 8, G −2 cm). At Bidart, the first weak central ridge is detected 12 cm below the K–Pg boundary (Fig. 8, B −12 cm). Similar to Gubbio, the "first appearance" central ridge has lower median coercivity, which indicates a predominant BS component. Such systematically lower coercivities may indicate the appearance of opportunistic magnetotactic bacteria (with a particular magnetosome morphology), or partial modification of the biogenic magnetite assemblage (ratio of collapsed versus intact chains). After the first appearance, biogenic magnetite production recovered fully at Bidart; samples from 4 and 2 cm below the K–Pg boundary have well-developed central ridge signatures similar to those of background Maastrichtian sediments (Fig. 8). The presence of biogenic magnetite, which is particularly sensitive to reductive dissolution, between the K–Pg boundary clay and the LSZ, is inconsistent with the downward percolation of reducing fluids as suggested by Lowrie et al. (1990). More likely, the LSZ marks a different environmental event that preceded the impact.

5.4. Origin of the LSZ

A strong decrease in detrital magnetite abundance relative to hematite in the LSZ is typical of the differential dissolution stability of iron oxides, while continuing formation of hematite pigment, particularly at Bidart, suggests a predominantly oxic environment and a continuing supply of reactive iron during deposition of LSZ sediments. Such a combination suggests that iron oxide dissolution occurred before the sediment was deposited. This unusual situation can be explained by the particular environmental conditions that prevailed at the time, where acidic weathering provides a plausible mechanism for iron oxide dissolution. Modelling of magnetite dissolution suggests that at a rainwater pH of 4.6 (lower than the "normal" present-day pH of ∼5.6), >90% of detrital magnetite would dissolve during transportation from the sediment source area to the deposition site (Font et al., 2014). Increased acidity of meteoric water is a common consequence of large aerosol release during volcanic eruptions. Detection of akaganeite – a rare chlorine-bearing iron oxyhydroxide – that occurs exclusively in the LSZ at Gubbio and Bidart (Font et al., 2011, 2014; Font and Abrajevitch, 2014) provides support for a volcanism-related origin of the LSZ. Large (∼5–40 μm) akaganeite crystals with plate-like, granular and semi-hexagonal morphologies isolated at Gubbio and Bidart are similar to those observed in aerosols of Masaya volcano, Nicaragua (Moune et al., 2010).

The most likely volcanic event responsible for LSZ formation below the K–Pg boundary is Phase 2 of Deccan volcanism, which represents >80% of the entire 3500-m-thick Deccan lava pile that erupted over <1 Myr (Chenet et al., 2007, 2008, 2009). U–Pb dating of zircons from the bole beds (intertrappean deposits) of the Ambenali section, western Ghats (India), indicates that the main eruptive phase initiated ∼250,000 yrs before the K–Pg boundary and that more than 1.1 million km^3 of basalts erupted in ∼750 kyr (Schoene et al., 2015). The onset of Deccan Phase 2 coincided with the CF1-CF2 interval (Keller et al., 2010; Keller, 2014) and, thus, is coincident with deposition of the LSZ interval. High CO_2 influxes and sulphuric acid aerosols from Deccan Phase 2 eruptions (Self et al., 2006; Chenet et al., 2007) are likely to have caused atmospheric acidification and iron oxide dissolution, and would have led to dramatic changes in marine environments, including extinctions of planktic foraminifera, nanno- and macro-fossils (e.g., Gertsch et al., 2011; Keller et al., 2010; Keller, 2014), and disruption of magnetofossil burial.

6. Conclusions

Detailed magnetic investigations are presented here for the Cretaceous–Paleogene transition in two complete classic stratigraphic sections: Gubbio (Italy) and Bidart (France). The sections have similar carbonate lithology, a boundary clay, and a distinct low susceptibility zone below the K–Pg boundary. However, they record different sedimentation patterns; bedded limestone with shale interbeds at Gubbio versus massive marls at Bidart. Comparison of magnetic characteristics of the limestone beds with those of the shale interbeds at Gubbio suggests that in addition to an order of magnitude difference in the bulk magnetic mineral content, the two lithologies differ systematically in biogenic magnetite content, with corresponding differences in the median grain-size of the low coercivity fractions. Distinctive biogenic signatures suggest that diagenetic processes affected the magnetic mineral assemblages of the two lithologies differently during periods of limestone and shale interbed deposition. To obtain an unbiased record

of environmental changes across the K–Pg boundary at Gubbio, we focus our magnetic interpretations on limestone beds.

Similar to previous studies of the Gubbio section, we detect a significant decrease in the total magnetic mineral content in the low susceptibility interval, with a larger loss of magnetite compared to hematite. The decreased detrital magnetite component is also observed at Bidart; however, unlike at Gubbio, magnetite loss is not accompanied by a decreased hematite content. Biogenic magnetite (magnetofossils) is present ubiquitously in background Maastrichtian and Danian samples from both sections, but it is absent in the low susceptibility intervals and reappears prior to the boundary clay that marks the K–Pg boundary. The presence of biogenic magnetite, which is particularly sensitive to reductive dissolution, below the boundary clay is inconsistent with the previously proposed model of low susceptibility zone formation due to downward propagation of reducing fluids in the aftermath of the asteroid impact (Lowrie et al., 1990). We conclude that the low susceptibility zone marks an environmental event that preceded the impact. The most likely cause of changing magnetic properties in the low susceptibility zone below the K–Pg boundary is an increase in atmospheric and oceanic acidity related to a high influx of volatiles from Phase 2 of Deccan Traps eruptions.

Acknowledgements

We gratefully acknowledge support from the Australian Research Council (ARC) through grant FS1001000076 to APR and colleagues that provided a Super Science Fellowship to AA, ARC grants LE120100218 and DP140104544, and FCT grant (PTDC/CTE-GIX/117298/2012) to EF. We thank Ramon Egli and Gerta Keller for constructive review comments.

References

Abrajevitch, A., Kodama, K., 2011. Diagenetic sensitivity of paleoenvironmental proxies: a rock magnetic study of Australian continental margin sediments. Geochem. Geophys. Geosyst. 12, Q05Z24. http://dx.doi.org/10.1029/2010GC003481.

Abrajevitch, A., Hori, R.S., Kodama, K., 2011. Magnetization carriers and remagnetization of bedded chert. Earth Planet. Sci. Lett. 305, 135–142.

Abrajevitch, A., Hori, R.S., Kodama, K., 2013. Rock magnetic record of the Triassic–Jurassic transition in pelagic bedded chert of the Inuyama section, Japan. Geology 41, 803–806.

Abrajevitch, A., Van der Voo, R., Rea, D.K., 2009. Variations in relative abundances of goethite and hematite in Bengal Fan sediments: climatic vs. diagenetic signals. Mar. Geol. 267, 191–206.

Alvarez, L.W., Alvarez, W., Asaro, F., Michel, H.V., 1980. Extraterrestrial cause for the Cretaceous–Tertiary extinction. Science 208, 1095–1108.

Archibald, J.D., Bryant, L.J., 1990. Differential Cretaceous/Tertiary extinctions of nonmarine vertebrates; evidence from northeastern Montana. Spec. Pap., Geol. Soc. Am., vol. 247, pp. 549–562.

Arenillas, I., Arz, J.A., Grajales-Nishimura, J.M., Murillo-Muñetón, G., Alvarez, W., Camargo-Zanoguera, A., Molina, E., Rosales-Domínguez, C., 2006. Chicxulub impact event is Cretaceous/Paleogene boundary in age: new micropaleontological evidence. Earth Planet. Sci. Lett. 249, 241–257.

Arthur, M.A., Fischer, A.G., 1977. Upper Cretaceous–Paleocene magnetic stratigraphy at Gubbio, Italy I. Lithostratigraphy and sedimentology. Geol. Soc. Am. Bull. 88, 367–371.

Baker, A.R., French, M., Linge, K.L., 2006. Trends in aerosol nutrient solubility along a west–east transect of the Saharan dust plume. Geophys. Res. Lett. 33, L07805. http://dx.doi.org/10.1029/2005GL024764.

Bathurst, R.G., 1972. Carbonate Sediments and their Diagenesis, vol. 12. Elsevier.

Bonté, P., Delacotte, O., Renard, M., Laj, C., Boclet, D., Jehanno, C., Rocchia, R., 1984. An iridium rich layer at the Cretaceous/Tertiary boundary in the Bidart section (southern France). Geophys. Res. Lett. 11, 473–476.

Carter-Stiglitz, B., Banerjee, S.K., Gourlan, A., Oches, E., 2006. A multi-proxy study of Argentina loess: marine oxygen isotope stage 4 and 5 environmental record from pedogenic hematite. Palaeogeogr. Palaeoclimatol. Palaeoecol. 239, 45–62.

Chang, L., Winklhofer, M., Roberts, A.P., Heslop, D., Florindo, F., Dekkers, M.J., Krijgsman, W., Kodama, K., Yamamoto, Y., 2013. Low-temperature magnetic properties of pelagic carbonates: oxidation of biogenic magnetite and identification of magnetosome chains. J. Geophys. Res. 118, 6049–6065. http://dx.doi.org/10.1002/2013JB010381.

Channell, J.E.T., Freeman, R., Heller, F., Lowrie, W., 1982. Timing of diagenetic haematite growth in red pelagic limestones from Gubbio (Italy). Earth Planet. Sci. Lett. 58, 189–201.

Chenet, A.L., Quidelleur, X., Fluteau, F., Courtillot, V., Bajpai, S., 2007. 40 K–40 Ar dating of the Main Deccan large igneous province: further evidence of KTB age and short duration. Earth Planet. Sci. Lett. 263, 1–15.

Chenet, A.L., Fluteau, F., Courtillot, V., Gerard, M., Subbarao, K.V., 2008. Determination of rapid Deccan eruptions across the Cretaceous–Tertiary boundary using paleomagnetic secular variation: results from a 1200-m-thick section in the Mahabaleshwar escarpment. J. Geophys. Res. 113, B04101. http://dx.doi.org/10.1029/2006JB004635.

Chenet, A.L., Courtillot, V., Fluteau, F., Gerard, M., Quidelleur, X., Khadri, S.F.R., Subbarao, K.V., Thordarson, T., 2009. Determination of rapid Deccan eruptions across the Cretaceous–Tertiary boundary using paleomagnetic secular variation: 2. Constraints from analysis of eight new sections and synthesis for a 3500-m-thick composite section. J. Geophys. Res. 114, B06103. http://dx.doi.org/10.1029/2008JB005644.

Cornell, R.M., Schwertmann, U., 2006. The Iron Oxides: Structure, Properties, Reactions, Occurrences and Uses. John Wiley & Sons.

Courtillot, V., Fluteau, F., 2010. Cretaceous extinctions: the volcanic hypothesis. Science 328, 973–974.

Crocket, J.H., Officer, C.B., Wezel, F.C., Johnson, G.D., 1988. Distribution of noble metals across the Cretaceous/Tertiary boundary at Gubbio, Italy: iridium variation as a constraint on the duration and nature of Cretaceous/Tertiary boundary events. Geology 16, 77–80.

Dekkers, M.J., 1989. Magnetic properties of natural goethite—II. TRM behaviour during thermal and alternating field demagnetization and low-temperature treatment. Geophys. J. Int. 97, 341–355.

Dekkers, M.J., 2007. Magnetic proxy parameters. In: Encyclopedia of Geomagnetism and Paleomagnetism. Springer, Netherlands, pp. 525–534.

Egli, R., 2004. Characterization of individual rock magnetic components by analysis of remanence curves. 3. Bacterial magnetite and natural processes in lakes. Phys. Chem. Earth 29, 869–884.

Egli, R., Chen, A.P., Winklhofer, M., Kodama, K.P., Horng, C.S., 2010. Detection of noninteracting single domain particles using first-order reversal curve diagrams. Geochem. Geophys. Geosyst. 11, Q01Z11. http://dx.doi.org/10.1029/2009GC002916.

Ellwood, B.B., MacDonald, W.D., Wheeler, C., Benoist, S.L., 2003. The K–T boundary in Oman: identified using magnetic susceptibility field measurements with geochemical confirmation. Earth Planet. Sci. Lett. 206, 529–540.

Fan, S.M., Moxim, W.J., Levy, H., 2006. Aeolian input of bioavailable iron to the ocean. Geophys. Res. Lett. 33, L07602. http://dx.doi.org/10.1029/2005GL024852.

Font, E., Abrajevitch, A., 2014. Paleoenvironmental signature of the Deccan Phase-2 eruptions. Earth Sci. Front. 2, 23.

Font, E., Fabre, S., Nédélec, A., Adatte, T., Keller, G., Veiga-Pires, C., Ponte, J., Mirão, J., Khozyem, H., Spangenberg, J.E., 2014. Atmospheric halogen and acid rains during the main phase of Deccan eruptions: magnetic and mineral evidence. Spec. Pap., Geol. Soc. Am., vol. 505. SPE505-18.

Font, E., Nédélec, A., Ellwood, B.B., Mirão, J., Silva, P.F., 2011. A new sedimentary benchmark for the Deccan Traps volcanism? Geophys. Res. Lett. 38, L24309. http://dx.doi.org/10.1029/2011GL049824.

France, D.E., Oldfield, F., 2000. Identifying goethite and hematite from rock magnetic measurements of soils and sediments. J. Geophys. Res. 105, 2781–2795.

Frankel, R.B., Bazylinski, D.A., Johnson, M.S., Taylor, B.L., 1997. Magneto-aerotaxis in marine coccoid bacteria. Biophys. J. 73, 994–1000.

Galbrun, B., Gardin, S., 2004. New chronostratigraphy of the Cretaceous–Paleogene boundary interval at Bidart (France). Earth Planet. Sci. Lett. 224, 19–32.

Gertsch, B., Keller, G., Adatte, T., Garg, R., Prasad, V., Berner, Z., Fleitmann, D., 2011. Environmental effects of Deccan volcanism across the Cretaceous–Tertiary transition in Meghalaya, India. Earth Planet. Sci. Lett. 310, 272–285.

Gulick, S.P.S., Christeson, G.L., Barton, P.J., Grieve, R.A.F., Morgan, J.V., Urrutia-Fucugauchi, J., 2013. Geophysical characterization of the Chicxulub impact crater. Rev. Geophys. 51, 31–52. http://dx.doi.org/10.1002/rog.20007.

Harris, S.E., Mix, A.C., 1999. Pleistocene precipitation balance in the Amazon Basin recorded in deep sea sediments. Quat. Res. 51, 14–26.

Heller, F., 1978. Rock magnetic studies of Upper Jurassic limestones from southern Germany. J. Geophys. 44, 525–543.

Heslop, D., Roberts, A.P., 2012. Estimation of significance levels and confidence intervals for first-order reversal curve distributions. Geochem. Geophys. Geosyst. 13, Q12Z40. http://dx.doi.org/10.1029/2012GC004115.

Heslop, D., Roberts, A.P., Chang, L., 2014. Characterizing magnetofossils from first-order reversal curve (FORC) central ridge signatures. Geochem. Geophys. Geosyst. 15, 2170–2179.

Hildebrand, A.R., Penfield, G.T., Kring, D.A., Pilkington, M., Camargo, A., Jacobsen, S.B., Boynton, W.V., 1991. Chicxulub crater: a possible Cretaceous/Tertiary boundary impact crater on the Yucatan Peninsula, Mexico. Geology 19, 867–871.

Johnsson, M.J., Reynolds, R.C., 1986. Clay mineralogy of shale-limestone rhythmites in the Scaglia Rossa (Turonian-Eocene), Italian Apennines. J. Sediment. Res. 56, 501–509.

Keller, G., 2014. Deccan volcanism, the Chicxulub impact, and the end-Cretaceous mass extinction: Coincidence? Cause and effect? Spec. Pap., Geol. Soc. Am., vol. 505, pp. 57–89.

Keller, G., Adatte, T., Pardo, A., Bajpai, S., Khosla, A., Samant, B., 2010. Cretaceous extinctions: evidence overlooked. Science 328, 974–975.

Keller, G., Li, L., MacLeod, N., 1996. The Cretaceous/Tertiary boundary stratotype section at El Kef, Tunisia: how catastrophic was the mass extinction? Palaeogeogr. Palaeoclimatol. Palaeoecol. 119, 221–254.

Keller, G., Barrera, E., Schmitz, B., Mattson, E., 1993. Gradual mass extinction, species survivorship, and long-term environmental changes across the Cretaceous–Tertiary boundary in high latitudes. Geol. Soc. Am. Bull. 105, 979–997.

Kobayashi, A., Kirschvink, J.L., Nash, C.Z., Kopp, R.E., Sauer, D.A., Bertani, L.E., Voorhout, W.F., Taguchi, T., 2006. Experimental observation of magnetosome chain collapse in magnetotactic bacteria: sedimentological, paleomagnetic, and evolutionary implications. Earth Planet. Sci. Lett. 245, 538–550.

Kruiver, P.P., Passier, H.F., 2001. Coercivity analysis of magnetic phases in sapropel S1 related to variations in redox conditions, including an investigation of the S ratio. Geochem. Geophys. Geosyst. 2 (12).

Kruiver, P.P., Dekkers, M.J., Heslop, D., 2001. Quantification of magnetic coercivity components by the analysis of acquisition curves of isothermal remanent magnetisation. Earth Planet. Sci. Lett. 189, 269–276.

Lefevre, C.T., Abreu, F., Schmidt, M.L., Lins, U., Frankel, R.B., Hedlund, B.P., Bazylinski, D.A., 2010. Moderately thermophilic magnetotactic bacteria from hot springs in Nevada. Appl. Environ. Microbiol. 76, 3740–3743.

Lefèvre, C.T., Frankel, R.B., Pósfai, M., Prozorov, T., Bazylinski, D.A., 2011. Isolation of obligately alkaliphilic magnetotactic bacteria from extremely alkaline environments. Environ. Microbiol. 13, 2342–2350.

Li, J., Pan, Y., Liu, Q., Yu-Zhang, K., Menguy, N., Che, R., Qin, H., Yang, X.A., 2010. Biomineralization, crystallography and magnetic properties of bullet-shaped magnetite magnetosomes in giant rod magnetotactic bacteria. Earth Planet. Sci. Lett. 293, 368–376.

Lin, W., Wang, Y., Pan, Y., 2012. Short-term effects of temperature on the abundance and diversity of magnetotactic cocci. MicrobiologyOpen 1, 53–63.

Liu, Q., Yu, Y., Torrent, J., Roberts, A.P., Pan, Y., Zhu, R., 2006. Characteristic low-temperature magnetic properties of aluminous goethite (α-(Fe, Al) OOH) explained. J. Geophys. Res. 111, B12S34. http://dx.doi.org/10.1029/2006JB004560.

Liu, S., Deng, C., Xiao, J., Li, J., Paterson, G.A., Chang, L., Yi, L., Qin, H., Pan, Y., Zhu, R., 2015. Insolation driven biomagnetic response to the Holocene Warm Period in semi-arid East Asia. Sci. Rep. 5. http://dx.doi.org/10.1038/srep08001.

Lowrie, W., Alvarez, W., Asaro, F., 1990. The origin of the white beds below the Cretaceous–Tertiary boundary in the Gubbio section, Italy. Earth Planet. Sci. Lett. 98, 303–312.

MacLeod, N., Rawson, P.F., Forey, P.L., Banner, F.T., Boudagher-Fadel, M.K., Bown, P.R., Burnett, J.A., Chambers, P., Culver, S., Evans, S.E., Jeffery, C., Kaminski, M.A., Lord, A.R., Milner, A.C., Milner, A.R., Morris, N., Owen, E., Rosen, B.R., Smith, A.B., Taylor, P.D., Urquhart, E., Young, J.R., 1997. The Cretaceous–Tertiary biotic transition. J. Geol. Soc. Lond. 154, 265–292.

Maher, B.A., 1988. Magnetic properties of some synthetic sub-micron magnetites. Geophys. J. 94, 83–96.

Marshall, C.R., Ward, P.D., 1996. Sudden and gradual molluscan extinctions in the latest Cretaceous of western European Tethys. Science 274, 1360–1363.

Molina, E., Alegret, L., Arenillas, I., Arz, J.A., Gallala, N., Hardenbol, J., von Salis, K., Steurbaut, E., Vandenberghe, N., Zaghbib-Turki, D., 2006. The Global Boundary Stratotype Section and Point for the base of the Danian Stage (Paleocene, Paleogene, "Tertiary", Cenozoic) at El Kef, Tunisia – original definition and revision. Episodes 29, 263–278.

Montanari, A., Hay, R.L., Alvarez, W., Asaro, F., Michel, H.V., Alvarez, L.W., Smit, J., 1983. Spheroids at the Cretaceous–Tertiary boundary are altered impact droplets of basaltic composition. Geology 11, 668–671.

Morin, F.J., 1950. Magnetic susceptibility of alpha-Fe_2O_3 and alpha-Fe_2O_3 with added titanium. Phys. Rev. 78, 819–820.

Moskowitz, B.M., Frankel, R.B., Bazylinski, D.A., Jannasch, H.W., Lovley, D.R., 1989. A comparison of magnetite particles produced anaerobically by magnetotactic and dissimilatory iron-reducing bacteria. Geophys. Res. Lett. 16, 665–668.

Moune, S., Gauthier, P.J., Delmelle, P., 2010. Trace elements in the particulate phase of the plume of Masaya Volcano, Nicaragua. J. Volcanol. Geotherm. Res. 193, 232–244.

Osete, M.L., Marcos, V.V., Ruiz, F.M., Lamolda, M.A., 2010. The Cretaceous–Tertiary boundary in the Iberian Peninsula marine record: meteoritic impact phases, diagenesis and paleoenvironmental effects deduced from rock magnetism. Fís. Tierra 22, 81–124.

Özdemir, Ö., Dunlop, D.J., Berquo, T.S., 2008. Morin transition in hematite: size dependence and thermal hysteresis. Geochem. Geophys. Geosyst. 9, Q10Z01. http://dx.doi.org/10.1029/2008GC002110.

Pechersky, D.M., 2008. Enrichment of sediments in iron hydroxides at the Mesozoic–Cenozoic boundary: a synthesis of petromagnetic data. Izv. Phys. Solid Earth 44, 232–238.

Pike, C.R., Roberts, A.P., Verosub, K.L., 1999. Characterizing interactions in fine magnetic particle systems using first order reversal curves. J. Appl. Phys. 85, 6660–6667.

Pike, C.R., Roberts, A.P., Verosub, K.L., 2001. First-order reversal curve diagrams and thermal relaxation effects in magnetic particles. Geophys. J. Int. 145, 721–730.

Poulton, S.W., Krom, M.D., Raiswell, R., 2004. A revised scheme for the reactivity of iron (oxyhydr)oxide minerals towards dissolved sulfide. Geochim. Cosmochim. Acta 68, 3703–3715.

Raup, D.M., Sepkoski, J.J., 1986. Periodic extinction of families and genera. Science 231, 833–836.

Renne, P.R., Deino, A.L., Hilgen, F.J., Kuiper, K.F., Mark, D.F., Mitchell, W.S., Morgan, L.E., Mundil, R., Smit, J., 2013. Time scales of critical events around the Cretaceous–Paleogene boundary. Science 339, 684–687.

Ricken, W., 1986. Diagenetic Bedding: A Model for Marl-Limestone Alternations. Lect. Notes Earth Sci., vol. 6. Springer Verlag, Berlin.

Roberts, A.P., Cui, Y., Verosub, K.L., 1995. Wasp-waisted hysteresis loops: mineral magnetic characteristics and discrimination of components in mixed magnetic systems. J. Geophys. Res. 100, 17909–17924.

Roberts, A.P., Pike, C.R., Verosub, K.L., 2000. First-order reversal curve diagrams: a new tool for characterizing the magnetic properties of natural samples. J. Geophys. Res. 105, 28461–28475.

Roberts, A.P., Florindo, F., Villa, G., Chang, L., Jovane, L., Bohaty, S.M., Larrasoaña, J.C., Heslop, D., Fitz Gerald, J.D., 2011. Magnetotactic bacterial abundance in pelagic marine environments is limited by organic carbon flux and availability of dissolved iron. Earth Planet. Sci. Lett. 310, 441–452.

Roberts, A.P., Florindo, F., Chang, L., Heslop, D., Jovane, L., Larrasoaña, J.C., 2013. Magnetic properties of pelagic marine carbonates. Earth-Sci. Rev. 127, 111–139.

Roberts, A.P., Heslop, D., Zhao, X., Pike, C.R., 2014. Understanding fine magnetic particle systems through use of first-order reversal curve diagrams. Rev. Geophys. 52, 557–602. http://dx.doi.org/10.1002/2014RG000462.

Robertson, D.J., France, D.E., 1994. Discrimination of remanence-carrying minerals in mixtures, using isothermal remanent magnetisation acquisition curves. Phys. Earth Planet. Inter. 82, 223–234.

Robin, E., Froget, L., Jéhanno, C., Rocchia, R., 1993. Evidence for a K/T impact event in the Pacific Ocean. Nature 363, 615–617.

Rocchia, R., Boclet, D., Bonte, P., Jehanno, C., Chen, Y., Courtillot, V., Mary, C., Wezel, F., 1990. The Cretaceous–Tertiary boundary at Gubbio revisited: vertical extent of the Ir anomaly. Earth Planet. Sci. Lett. 99, 206–219.

Salazar, A., Morales, A., Marquez, M., 2011. Characterization of natural microcosms of estuarine magnetotactic bacteria. Dyna 78, 72–80.

Schoene, B., Samperton, K.M., Eddy, M.P., Keller, G., Adatte, T., Bowring, S.A., Khadri, S.F.R., Gertsch, B., 2015. U–Pb geochronology of the Deccan Traps and relation to the end-Cretaceous mass extinction. Science 347, 182–184.

Schulte, P., Alegret, L., Arenillas, I., Arz, J.A., Barton, P.J., Bown, P.R., Bralower, T.J., Christeson, G.L., Claeys, P., Cockell, C.S., Collins, G.S., Deutsch, A., Goldin, T.J., Goto, K., Grajales-Nishimura, J.M., Grieve, R.A.F., Gulick, S.P.S., Johnson, K.R., Kiessling, W., Koeberl, C., Kring, D.A., MacLeod, K.G., Matsui, T., Melosh, J., Montanari, A., Morgan, J.V., Neal, C.R., Nichols, D.J., Norris, R.D., Pierazzo, E., Ravizza, G., Rebolledo-Vieyra, M., Reimold, W.U., Robin, E., Salge, T., Speijer, R.P., Sweet, A.R., Urrutia-Fucugauchi, J., Vajda, V., Whalen, M.T., Willumsen, P.S., 2010. The Chicxulub asteroid impact and mass extinction at the Cretaceous–Paleogene boundary. Science 327, 1214–1218.

Schwertmann, U., Murad, E., 1983. Effect of pH on the formation of goethite and hematite from ferrihydrite. Clays Clay Miner. 31, 277–284.

Self, S., Widdowson, M., Thordarson, T., Jay, A.E., 2006. Volatile fluxes during flood basalt eruptions and potential effects on the global environment: a Deccan perspective. Earth Planet. Sci. Lett. 248, 518–532.

Sharpton, V.L., Burke, K., Camargo-Zanoguera, A., Hall, S.A., Lee, D.S., Marin, L.E., Suáarez-Reynoso, G., Quezada-Muñeton, J.M., Spudis, P.D., Urrutia-Fucugauchi, J., 1993. Chicxulub multiring impact basin: size and other characteristics derived from gravity analysis. Science 261, 1564–1567.

Smit, J., 1999. The global stratigraphy of the Cretaceous–Tertiary boundary impact ejecta. Annu. Rev. Earth Planet. Sci. 27, 75–113.

Tauxe, L., Mullender, T.A.T., Pick, T., 1996. Potbellies, wasp-waists, and superparamagnetism in magnetic hysteresis. J. Geophys. Res. 101, 571–583.

Thibault, N., Gardin, S., 2010. The calcareous nannofossil response to the end-Cretaceous warm event in the Tropical Pacific. Palaeogeogr. Palaeoclimatol. Palaeoecol. 291, 239–252.

van der Zee, C., Roberts, D.R., Rancourt, D.G., Slomp, C.P., 2003. Nanogoethite is the dominant reactive oxyhydroxide phase in lake and marine sediments. Geology 31, 993–996.

Verma, H.C., Upadhyay, C., Tripathi, A., Tripathi, R.P., Bhandari, N., 2002. Thermal decomposition pattern and particle size estimation of iron minerals associated with the Cretaceous–Tertiary boundary at Gubbio. Meteorit. Planet. Sci. 37, 901–909.

Westphal, H., 2006. Limestone-marl alternations as environmental archives and the role of early diagenesis: a critical review. Int. J. Earth Sci. 95, 947–961.

Westphal, H., Hilgen, F., Munnecke, A., 2010. An assessment of the suitability of individual rhythmic carbonate successions for astrochronological application. Earth-Sci. Rev. 99, 19–30.

Yamazaki, T., 2012. Paleoposition of the Intertropical Convergence Zone in the eastern Pacific inferred from glacial–interglacial changes in terrigenous and biogenic magnetic mineral fractions. Geology 40, 151–154.

Zhang, Y.G., Ji, J., Balsam, W.L., Liu, L., Chen, J., 2007. High resolution hematite and goethite records from ODP 1143, South China Sea: co-evolution of monsoonal precipitation and El Niño over the past 600,000 years. Earth Planet. Sci. Lett. 264, 136–150.